CHEMISTRY & SUSTAINABILITY
CHEMSUSCHEM
ENERGY & MATERIALS

Accepted Article

Title: Tuning cobalt and nitrogen co-doped carbon to maximum catalytic sites by superabsorbent for efficient oxygen reduction

Authors: Mengran Liu, Hai Lin, Zongwei Mei, Jinlong Yang, Jie Lin, Yidong Liu, and Feng Pan

To be cited as: *ChemSusChem* 10.1002/cssc.201801480

Link to VoR: http://dx.doi.org/10.1002/cssc.201801480

A Journal of
ChemPubSoc Europe

WILEY-VCH www.chemsuschem.org

WILEY-VCH

DOI: 10.1002/ ((cssc.201801480R1))
Article type: Full Paper

Tuning cobalt and nitrogen co-doped carbon to maximum catalytic sites by superabsorbent for efficient oxygen reduction

Mengran Liu, Hai Lin, Zongwei Mei, Jinlong Yang, Jie Lin, Yidong Liu, and Feng Pan**

M. Liu, H. Lin, Dr. Z. Mei, Dr. J. Yang, Prof. Y. Liu, Prof. F. Pan
School of Advanced Materials, Peking University Shenzhen Graduate School, Shenzhen 518055, China.
E-mail: liuyd@pkusz.edu.cn (Y. Liu); panfeng@pkusz.edu.cn (F. Pan)
J. Lin
Fujian Institute of Subtropical Botany, Xiamen 361006, China

Keywords: transition metal-nitrogen doping carbon catalysts, oxygen reduction reaction, superabsorbent resin, cobalt content

The electrocatalytic performance and cost of oxygen reduction reaction (ORR) catalysts are crucial to many renewable energy conversion and storage systems/ devices. Recently, transition metal-nitrogen doping carbon catalysts (M-N-C) have attracted tremendous attention, which are effective to reduce costs and exhibit excellent catalytic activities, but are restricted in large-scale commercial applications by complex preparation processing. Here, a novel and facile strategy to prepare Co-N-C catalyst is developed. A kind of super absorbent resin normally found in diaper, poly (acrylic acid-acrylamide), is used to adsorb transition metal cobalt salt and followed pyrolysis strategy at 800 ℃ under argon atmosphere. The resin plays a multiple role simultaneously, including structural support, dispersing cobalt ions by coordinate bonds, providing carbon & nitrogen source and so on. Attributed to the conductive carbon frameworks and abundant catalytic sites, the Co-N-C catalyst exhibits excellent electrocatalytic performance. High onset potential (0.96 V vs. reversible hydrogen potential, RHE) and half-wave potential (0.80 V vs. RHE) and a large diffusion-limited current density (4.65 mA cm^{-2}) are achieved for ORR, comparable or superior to the commercial 20% Pt/C and reported M-N-C ORR electrocatalysts. This work provides a universal dispersion technology for Co-N-C catalyst, which makes it a very promising candidate toward ORR.

1. Introduction

Oxygen reduction reaction (ORR) is a critically important reaction in many renewable energy conversion and storage systems/ devices, such as fuel cells, metal-air batteries,[1] and some industrial processes like chlor-alkali electrolysis.[2] Nevertheless, due to the inherently sluggish kinetics of ORR compared with that of anodic reaction, it dramatically limits the energy conversion efficiency and turns to be the bottleneck to develop these energy devices.[3]

Currently, the state-of–the-art catalysts for ORR are still noble metal catalysts especially platinum (Pt) catalysts owing to low overpotentials and large current densities.[3a] However, these noble metal catalysts suffer from low earth reserves, high cost, poisoning effects and insufficient stability that severely limit their large-scale commercialization development.[4] In view of this, extensive research efforts have been carried out to overcome above problems, including noble metal-transition metal (such as Fe, Co, Cu and Ni) alloy with special structure control[4a, 5] and entirely new non-noble metal materials doped with the active elements, such as metal-free heteroatom-doped carbon materials,[1c, 6] transition metal-nitrogen doping carbon materials (M-N_x-C),[7] transition metal nitrides,[8] oxides,[9] sulfides,[10] as well as their hybrids[7b, 11] etc. Generally, there have been a series of techniques to prepare above catalysts which are mainly divided into two aspects.[12] The major one is the thermal treatment strategy of precursors with the help of sol-gel technique,[13] template method[14] and in situ synthesis,[15] etc. And the other one focuses on new strategies, involving chemical vapour deposition,[16] the wet-chemical strategy,[17] microwave method,[18] etc.

Among above new-type catalysts, the M-N_x-C (M =Fe and/or Co) catalysts are believed to be the most promising candidates for cathode catalysts recently.[19] Particularly, carbon materials with high electron conductivity, excellent corrosion resistance and tunable surface properties make them good supporters for active sites.[3a,

[20] Normally, The M-N_x-C catalysts are synthesized by thermal treatment of precursors at certain temperature in an inert environment (nitrogen or argon).[21] Upon pyrolysis, structure and morphology get changed and active sites for ORR are formed. Although the catalytic mechanism of this kind of catalysts is still under debate, it is obviously that the formation of the ORR active sites strongly depends on the composition of precursor.[19] Since 1964, Jasinski reported that cobalt phthalocyanine could work in catalyzing the ORR,[22] a lot of N-containing precursors with transition metal have been studied, which contain phthalocyanine,[23] porphyrin,[24] corrole,[25] polyacrylonitrile,[26] polypyrrole,[27] polyaniline[28] and polymerizable ionic liquid[29] etc. Among these N-containing precursors, it is particularly difficult and complex for the regulation of nitrogen content and the formation of nitrogen functional active groups with metal and carbon atoms.

Here in, we develop a novel one-step synthesis and followed pyrolysis method to prepare Co-N_x-C catalysts. By using inexpensive super absorbent resin poly (Acrylic acid-Acrylamide) (Poly (AA-AM)) to absorb cobalt salt solution (Co^{2+}@ Poly (AA-AM)), the aims of high level dispersion spontaneously, structural support without additional template and easy doping were achieved in one step. Pyrolysis of as-prepared Co^{2+}@ Poly (AA-AM) was carried out at 800 ℃ under argon atmosphere. Poly (AA-AM) not only plays a role in providing ligands, but also helps to achieve structural support easily because of the existence of cross-linked networks. On the other hand, due to the presence of amino and carboxyl groups, the transition metal ions are selectable, and the ratio of acrylic and acrylamide monomers can also be used to regulate the nitrogen content of the precursor. Although there are no pyridinium moieties and the ringforming structure on the Poly (AA-AM) molecule chain, it can be self-assembled with transition metal ions. After pyrolysis, it was confirmed that pyridinic N was formed to achieve excellent electrocatalytic performance. The obtained Co-N-C catalysts show flake

morphology with a high surface area of ~500 m^2 g^{-1}, uniform distribution of Co-N species, and certain nitrogen doping content in a continuous carbon framework. Our Co-N/C catalysts display superior ORR performances but extremely low cost compared to most of other ORR electrocatalyst, with a positive half-wave potential of 0.80 V versus reversible hydrogen electrode (RHE). As a whole, the ratio of N atom in the precursors used in our work is the smallest, but the catalytic performance is equal to or better than the other works. It shows that the utilization of nitrogen atoms is higher and high proportion of doping can be achieved.

2. Results and discussion

FT-IR spectra of pure hydrogels Poly (AA-AM) and Co^{2+}@Poly (AA-AM) are presented in **Figure 2a**. Several distinct characteristic absorption peaks can be clearly identified from the spectrum of pure hydrogels, confirming the copolymerizat-ion of AA and AM. Especially, the two peaks locate at 1650 cm^{-1} (the absorption peak of carbonyl group C=O connected to the amide group -$CONH_2$) and 1546 cm^{-1} (carbonyl group antisymmetric stretching vibration peak of -COO^-) respectively, suggest the existence of the amido groups and the carboxylic groups in the crosslinking network, which are hydrophilic groups. When hydrogels were added to the cobalt acetate solution, those ionizable groups on the network chain ionized in solution, in consequence, the positive ions existed as free-form, while the negative ions still were connected with network chain. These similarly charged adjacent groups repelled each other, and then the network expanded, providing space for water molecules and cobalt ion freely access to crosslinking network. Obviously, the two characteristic peaks mentioned above of Co^{2+}@Poly (AA-AM) shifted towards lower wavenumbers, about 30 cm^{-1}, compared with those of pure hydrogels Poly (AA-AM). This is due to Co^{2+} formed ionic bonds with -COO^- group and formed a stable complexing structure with -$CONH_2$, which promote the uniform distribution and stability of cobalt ions in hydrogels. In this work,

hydrogels serving as a superb template that contains rich the group of -COO^- and -$CONH_2$ play a significant role on providing structural support and prompting cobalt ions dispersing.

The pyrolysis of as-prepared Co^{2+}@Poly (AA-AM) was performed at high temperature in an inert atmosphere to complete the transformation of the organic to inorganic phase. The TGA/DSC tests were carried out to study the thermal decomposition performance of Co^{2+}@ Poly (AA-AM). In the range of low temperature, moisture in the sample volatilizes gradually. As the temperature rises, the organic groups and other small molecules are heated and decomposed violently in the inert atmosphere. When the temperature rises above the carbonization temperature, the non-carbon atoms were gradually eliminated, and the carbon atoms were further enriched and crosslinked. As the DSC curve of Co^{2+}@Poly (AA-AM) complex depict (**Figure S1**), an obvious endothermic peak is observed at about 750 ℃, which might be a result of the formation of carbonaceous framework.[14b]

Overall, the high ORR catalytic performance is in close connection with the surface property, the elemental composition and their interaction of the catalysts, for instance, a high active site density, a proper porosity to facilitate mass transport, and a high degree of carbonization to achieve high electrical conductivity are essential parameters.[30]

XRD patterns of 800-2 and 800-5 Co-N-C catalysts are displayed in **Figure 2b**. No obvious characteristic peak is observed in the XRD pattern of 800-2 Co-N-C, which might result from the formation of amorphous structures or small crystal grains. However, with the increase of cobalt content, the crystal structure of Co-N-C catalysts get changed. The diffraction peaks at 44.2 º, 51.5 º, 75.9 º are attributed to the (111), (200) and (220) planes of metallic Co (PDF#15-0806), respectively. Besides, the characteristic peaks at 31.3 º and 38.6 º are ascribed to the (220) and (222) plane of Co_3O_4 phase (PDF#43-1003), implying the formation of Co-O moieties. From the results, we suspect that during pyrolysis process, cobalt atoms congregate first to form metal nanoclusters, and then the rising cobalt content leads to the increasing size

of crystal, in the meantime, oxygen atoms would participate in for the further formation of Co-O structure.

SEM and TEM images are acquired to investigate the morphologies and microstructures of the catalysts. After the pyrolysis treatment and ball milling, highly carbonized carbonaceous layer stacked up to particles with an open porous structure was formed. These particles have a diameter range from about 100 nm to 2 μm (**Figure 3a, b**). To take further insights into the surface area and porosity of the catalysts, N_2 sorption isotherms of 800-0, 800-2 and 800-5 Co-N-C catalysts were characterized (**Figure 2d**). All samples exhibited sharp uptakes at a relatively low N_2 partial pressures (<0.01) indicating the existence of micropores (<2 nm).[26] while 800-2 Co-N-C also showed a well-defined hysteresis loop at higher N_2 pressures (from 0.4 to 1.0), which classed as a typical type IV isotherm, suggesting the existence of mesopores as well.[9] The BET specific surface areas show an increase from 315.83 $m^2 g^{-1}$ to 496.85 $m^2 g^{-1}$. The largest surface area and porosity of 800-2 probably attributes to the well-distributed cobalt element, which plays a catalytic part in carbonization and the formation of N-C doping. High-resolution TEM (HRTEM) of 800-2 Co-N-C (**Figure 3c**) shows that small nanoclusters (observed easily in the edge area and marked by yellow circles) with a narrow size distribution about 2-5 nm were embedded in the carbon support uniformly. [14b] As magnified insert in **Figure 3c**, these nanoclusters show the lattice spacing of 0.214 nm, which is slightly larger compared with the standard value of the (111) plane of metallic Co. We speculated that the larger lattice space may result from the intercalation of nitrogen, oxygen and/or carbon into the cobalt spaces.[31] The carbonaceous fringes with a d-spacing of 0.352 nm correspond to the (002) plane of graphitic carbon. **Figure 3d** shows the HR-TEM image of 800-5 Co-N/C. The lattice spacing marked at A/B/C in this figure is 0.208 nm, 0.176 nm, and 0.125 nm, corresponding to the (111) (200) (220) crystal face of metallic cobalt respectively. But the grain size is much larger than that in 800-2. Besides, the lattice spacing presented at D/E is 0.243 nm and 0.286 nm, corresponding to the (220) (222) plane of Co_3O_4 respectively. Above

information obtained from HRTEM images is consistent with XRD patterns. To further investigate the elemental distribution of Co element in the catalyst, HAADF-STEM (**Figure 3e**) and HAADF-STEM-EDS mappings (**Figure 3g**) of 800-2 Co-N-C were conducted. As displayed in **Figure 3e**, the bright dots with relative light contrast correspond to Co atoms, while the carbonized support materials with dark contrast. From HAADF-STEM-EDS mappings of the edge area (**Figure 3g and Figure S2**), the catalysts are mainly composed of C, O, N, and Co elements. The major elements C and N are evenly distributed, while the distributions of O and Co elements with relatively low proportion are correlated and interactive clearly, informing that O atoms and nitrogen-doped carbon fragments probably grabbed around Co containing structure.

The surface chemical composition and state of Co-N-C were further characterized by XPS as shown in **Figure 4**. The survey spectrum (shown in **Figure 4a** and detailed parameters in **Table S1**&**S2**) reconfirms the presence of C, N, O and Co elements contained in Co-N-C catalysts. When the pyrolysis temperature rising from 700 ℃ to 800 ℃, these catalysts show an increase in C atomic contents, but a decrease in N and O contents, and almost invariant Co atomic contents. When further rising up to 900 ℃, the sharp decrease in cobalt content may be due to the fact that cobalt atoms are congregated together and blocked by surface carbon shells, therefore, some Co atoms cannot be detected by XPS. Simultaneously, C atomic content still presents a trend of slight increase. The results can inform that the higher carbonization degree is obtained at higher temperature, which is further enhanced the electrical conductivity of these catalysts.[12]

The high-resolution C 1s spectra (**Figure S3**) of the catalysts are deconvoluted into five peaks, indicating the presence of different carbon species: C=C (284.43 eV), C-C (284.88 eV), C=O/C-N (286.20 eV), C-O/C=N (288.10 eV) and π-π (289.50 eV). The dominant carbon specie of the 800-2 Co-N-C- is C=C bonding in sp^2 hybridization (284.43 eV), while at the higher binding energy, 286.20 eV and 288.10 eV, carbon atoms are bound to more

electronegative heteroatoms. As a result, the electron density of these carbon atoms is lower. The formed C^+ is believed to promote dissociative adsorption of oxygen, leading to four-electron reduction pathway of ORR.[6] Overall, with the pyrolysis temperature increases, the percentages of C=C bonds increases as well, while C=O/C-N shows a decrease, indicating a higher carbonization (the detailed parameters in **Table S3**). Besides, there is no clear peak corresponding to a carbon atom bound to a Co atom, implying the absence or low content of cobalt carbide species, which is in good agreement with the XRD and the later Co 2p analysis results.

The formation of the Co-N bonds can be confirmed by the fitted high resolution N1s XPS spectra with an asymmetrical shape, as shown in **Figure 4c**. There are mainly three types of the nitrogen species: pyrrolic N (400.1 eV), metal-coordinated Co-N_x (399.2 eV), and pyridinic N (398.5 eV). Pyridinc-N exists at the edge of graphite plans, and the nitrogen atom bonds to two carbon atoms, containing a lone electron pair, which can enhance the electron-donor or basic capacities of the carbon materials. Thereby, it can effectively improve the adsorption capacity of O_2 and onset potential for the ORR.[32] Besides, weak significant contribution at high binding energy value of more than 401 eV (401.2eV for graphitic N, and 404 eV for oxidized N), indicating that there are seldom nitrogen atoms that truly replace the carbon atoms in graphene-sheet binding conditions or band to O atoms directly, ascribed to polymer precursor Poly (AA-AM). From the fitted high resolution N1s XPS spectrums of 800-(0/5) Co-N-C (**Figure S4**), with the addition of cobalt content, the main peak gradually shifted to low binding energy, implying the increase of the percentage of pyridinic N in the total amount of N species. Recent studies reported that both pyridinic nitrogen and Co-N_x were found to have ORR catalytic activity. Therefore, the enhanced catalytic activity for the ORR observed on the Co-N-C catalyst should be attributed to the formation of pyridinic nitrogen and Co-N_x in the process of high-temperature pyrolysis.[33]

High-resolution Co 2p spectra consist of Co 2p1/2, Co 2p3/2 and their corresponding satellites. Overall, these two main peaks of 800-2 Co-N-C catalyst (797.50 eV for Co 2p1/2 &782.30 eV for Co 2p3/2) are separated by 15.2 eV, suggesting the mixed valence state of Co. Compared to 800-2, the two peaks of Co 2p1/2 and Co 2p3/2 of 700-2 Co-N-C are separated by 15 eV, confirming the only valence state (**Figure S5**). Obviously, as the cobalt content rises, the peak intensity of the Co 2p spectra increases, and the peak position gradually shifts toward the lower binding energy. In detail, the high-resolution Co 2p3/2 spectra of 800-5 Co-N-C catalyst is deconvoluted into three sharp peaks at about 779.59, 780.72 and 782.30 eV, attributed to metallic Co, Co_xO_y and Co-N_x, respectively. Compared to 800-5, the absence of metallic Co peak at 779.59 eV of 800-2 suggests that no or little inactive Co aggregates are formed. Furthermore, the largest percentage based on peak areas of Co-N_x species is observed at 800-2, which is considered to be one of the most effective catalytic sites for ORR.

Raman spectra of the catalysts are shown in **Figure 1d** & **Figure S7**. There are two strong peaks at 1350 cm^{-1} and 1597 cm^{-1}.These two peaks are assigned to the D band (1350 cm^{-1}) and G band (1597 cm^{-1}) of carbon, as D band is relative to the disorder and bonding between heteroatom and carbon, while G band arises from the in-plane vibration of the sp^2 carbon network.[3a] The ratio of the D band and G band I_D/I_G is generally adopted to detect the graphitization and disorder of carbon materials. The I_D/I_G of catalysts Co-N-C-800 increase with the addition of cobalt from 0.98 to 1.03 (**Figure 1d**), implying the higher disordered and richer defects in carbon matrix of the catalysts with a higher cobalt content. The results are fully consistent with the XPS findings. Moreover, the I_D/I_G of catalysts 700/800/900-2 Co-N-C decrease from 1.04 to 0.98 (**Figure S7**) with the pyrolysis temperature increasing, indicating that a higher pyrolysis temperature can contribute to a higher graphitization degree. Moreover, a small peak located at 672 cm^{-1} demonstrates the existence of Co_3O_4,[34] consistent with the results of XRD and HRTEM.

To investigate the electrocatalytic activity of as-prepared catalysts, CV measurements were first conducted at 10 mV s^{-1} in N_2 or O_2-saturated 0.1M KOH electrolytes. Comparing to the result that no significant response occurs in N_2-saturated solutions, a well- defined cathodic peak near 0.80 V versus RHE is observed in O_2-saturated electrolytes, implying an effective ORR electrocatalytic activity of Co-N-C catalysts **(Figure 5a)**. Furthermore, the LSV curves of 800-(0-5) Co-N-C are depicted in **Figure 5b** and the ORR performance parameters of catalysts are displayed in **Table 1**. Overall, the catalysts with relatively low cobalt doped exhibit better ORR activity with the similar positive onset potential around 0.96 V (800-1, 800-2, 800-3) and the half-wave potential $E_{1/2}$ of 0.80 V (800-1, 800-2). Especially, the most positive E_{onset} and the most positive $E_{1/2}$ of Co-N-C catalysts were 30 mV less and only 60 mV less than those of commercial 20% Pt/C respectively. Moreover, those parameter values exceed some M−N−C catalysts or other kinds of catalysts with much higher costs reported in the literature (as shown in **Table S4** & **5** & **6 & 7**). The obtained diffusion-limited current density of the 800-2 Co-N-C catalyst is 4.65 mA cm^{-2}, even larger than that of the commercial 20% Pt/C (4.64 mA cm^{-2}).

The 800-0 Co-N-C catalyst without any Co doping shows a relatively limited catalytic activity, then the catalytic activity is promoted continuously alongside Co doping up to wt.2%. An obvious enhanced diffusion-limited current density and a positive sifted the half-wave potential $E_{1/2}$ can be easily observed. However, with further increasing of Co content, ORR catalytic activity of Co-N-C catalysts show a trend of decreasing. Accurately, the effect of Co doping content on ORR catalytic activity is similar to a mountain plot as shown in the insert in **Figure 5b**, which is in good agreement with the above material characterization results. Combined with XPS analysis results, it can be concluded that Co−N species and pyridinic N play a catalytic role in favoring oxygen reduction reaction. When the cobalt content exceeds the optimized content, there will be a decrease in catalytic activity which is attributed to the formation of inactive cobalt aggregation species, metal cobalt and cobalt oxide, verified by

XRD results. Moreover, increasing the cobalt content also enhance the surface area and porosity, which is conducive to the exposure of metal-based active sites onto the surface, as well as the absorption and diffusion of molecular oxygen. Besides the percentages of Co elements, the pyrolysis temperature is one of the other critical synthesis parameters for the electrocatalysts. To further investigate the effect of pyrolysis temperature from 700 to 900 ℃ on ORR catalytic activity, as-precursors were fixed in the optimum Co doping content. **Figure S8** presents the LSV curves of 700/800/900-2 Co-N-C catalysts. Compared to 800-2 Co-N-C and 900-2 Co-N-C, the catalytic activity of 700-2 Co-N-C is negligible. According to above analysis section, it is proved that there is no sign of the formation of Co-N bonds (**Figure S5 & S6**). On the other hand, 700-2 Co-N-C is endowed with a slight poor electric conductivity due to the existence of a certain amount of oxygen-contained groups and the halfway carbonization. When the temperature rises to 900 ℃, the electrocatalysis performance of 900-2 Co-N-C catalyst would be affected by the removal of nitrogen elements. To gain a deep understanding of the reaction kinetics and pathways, the polarization curves of 800-2 Co-N-C were measured at various rotating rates ranging from 200 rpm to 1600 rpm, as shown in **Figure 5c**. The onset potentials remain constant while the current densities increase along with the increasing rotating rates, implying the kinetics-controlled of the ORR process. According to the Koutecky–Levich (K-L) equation, the corresponding K–L plots under various potentials of 800-2 Co-N-C were obtained by transforming the RDE data. Obviously, all of them exhibit excellent linearity (the inset of **Figure 5c**), suggesting the first-order reaction kinetics of the ORR toward the concentration of dissolved oxygen. As is known, the electrocatalytic reduction of O_2 in aqueous electrolytes goes through two generally recognized pathways, two electron pathways or four electron pathways.[30] The number of electrons transferred per oxygen molecule n was calculated about 3.89 based on the slope of K–L plots, suggesting a near-four-electron oxygen reduction process. Furthermore, the durability of 800-2 Co-N-C was also measured. After 2000 continuous cycles (**Figure 5d**), no obvious changes

happen to the $E_{1/2}$ and E_{onset}, while the diffusion-limited current density exhibited a little degradation about 7%, implying the stability of the active site requires being further improved. In addition, the ratio of AM/AA is a vital parameter of super absorbent resin serving as precursor of nitrogen and carbon source in this work, which may also influence the electrocatalytic properties of Co-N-C catalysts. Therefore, it is worth to further study in the next work.

Based on above experimental results, a possible mechanism was proposed to demonstrate the super catalytic activity of 800-2 Co-N-C catalyst. It is supposed that the pyridinic nitrogen and nitrogen-coordinated Co serve as catalytic active sites. On one hand, suitable pyrolysis temperature is mainly beneficial to guarantee a higher carbonization level and an optimal element proportion. Especially, 800 ℃ is the minimum temperature to form nitrogen-coordinated Co. On the other hand, the appropriate introduction of Co not only offers nitrogen-coordinated Co active sites, but also contributes to promote the N-doping, porous structure, and specific surface area of catalysts.[3a]

3. Conclusion

In summary, we developed an effective dispersing technology using super absorbent resin adsorbing metal ion and followed pyrolysis strategy to fabricate Co-N-C catalyst for ORR. The resin provides framework as well as doping elements sources to coordinate with metal ions to form actives sites. In this work, Poly (AA-AM) and cobalt were chosen to realize the idea. A large number of functional groups, amino and carboxyl, not only provide N and O, but also contribute to form nitrogen-doped carbon species and nitrogen-coordinated Co active sites. The Co-N-C catalyst exhibits excellent electrocatalytic performance which is comparable to the commercialized Pt/C catalyst, but the cost is far below it, which makes the composite catalyst easy to achieve commercialization instead of Pt-based catalyst. Also the formula could be modified, that various resins and metal ions provide huge amount of

possible couples makes the molecular level dispersion technology kind of universal and can be applied to other related fields.

4. Experimental Section

4.1. Chemicals and reagents

Cobalt (II) acetate tetrahydrate ($C_4H_6O_4Co \cdot 4H_2O$), methanol (MeOH) and KOH were purchased from National reagent (Shanghai, china). Isopropylalcohol [$(CH_3)_2CHOH$] was purchased from Fuyu reagent (Tianjin, China). Nafion solution (DuPont D520, 5%) and commercial Pt/C (20%) (Johnson Matthey catalysts) used as a standard catalyst was purchased from Hesen Company (Shanghai, China). All reagents were analytical grade and deionized water was used throughout this study.

4.2. Characterization

Fourier transform infrared spectrum (FT-IR) of Poly (AA-AM) superabsorbent resin was verified by a Perkin Elmer Frontier spectrophotometer. The thermogravimetry and differential scanning calorimetry (TGA/DSC) tests were measured using TGA/DSC simultaneous thermal analyser (TGA/DSC 1, Swiss Mettler Toledo). X-ray diffraction (XRD) patterns were carried on X-ray diffractometer (D8 Advance, Bruker) using silicon substrate without diffraction peak. The surface area and porosity of the Co-N-C catalysts were characterized by N_2 sorption isotherms using an Accelerated Surface Area and Porosimetry System (ASAP 2020 HD88, Micromeritics). Morphology and structure of the as-prepared Co-N-C were observed by the field emission scanning electron microscope (FESEM) (ZEISS SUPRA® 55, Carl Zeiss, Germany). Transmission electron microscopy (TEM) images were obtained from the TEM (JEM–3200FS, Japan).An Energy Dispersive Spectrometer (EDS) was used in the meanwhile. Raman Spectra were recorded on an in Via Raman Microscope (iHR320, Horiba, Japan). X-ray photoelectron spectrum (XPS) measurements were performed at an ESCALAB 250X X-ray Photoelectron Spectrometer (ESCALAB 250X, Thermo Fisher, England).

4.3. Electrode Preparations

To prepare the catalyst ink for electrochemical analysis, 10 mg of catalytic powders were dispersed in a mixed solution containing 100 μL Nafion solution (5 wt %), 400 μL isopropylalcohol and 1.5 mL deionized water. Subsequently, the mixed solution was sonicated for 20 min to form a homogeneous catalytic ink. Finally, 10 μL of catalytic ink was dropped on a glassy carbon disk electrode (0.196 cm^2). After being dried at ambient temperature, the catalyst with a content of 0.25 mg cm^{-2} was loaded on the working electrode. As a comparison, a Pt/C (20 wt. %) electrode was obtained with the similar method. The loading content of Pt/C on the electrode and the test conditions are consistent with Co-N-C samples.

4.4. Electrochemical Measurements

To investigate the ORR activities of the as-prepared catalysts, a series of electrochemical tests, including cyclic voltammetry (CV) and linear sweep voltammetry (LSV), were measured. All electrochemical measurements were performed on SHANGHAI CHENHUA CHI760D/E electrocatalytic workstation attached with a rotating disk electrode (RDE). The whole testing process was executed in a normal three-electrode system at room temperature, choosing a glassy carbon electrode modified with various electrocatalysts as the working electrode, a Pt wire as the counter electrode, and an Ag/AgCl (in 3 M KCl solution) electrode as the reference electrode.

Herein, 0.1 M KOH aqueous solution was used as the electrolyte and deaerated by high purity O_2 or N_2 according to concrete conditions throughout the testing process. CV experiments were recorded with a scan rate of 10 mV s^{-1}. LSV experiments were executed at 10 mV s^{-1} under rotating speeds varying from 200 to 1600 rpm. All the potentials in this work were referred to the reversible hydrogen electrode (RHE), E (RHE) = E (Ag/AgCl) + 0.976V.

Different publications give diverse definitions of the onset potential (E_{onset}) of ORR. It is defined as the potential value corresponding to 5% of the diffusion-limited current density (j_L) in this work.[2a] The mass activity was calculated by normalizing the kinetic-limiting current

density (j_K) to the mass of active materials. The kinetics parameters were obtained from the mass-transport corrected polarization curve though the Levich-Koutechky equation (**Equation 1**):

$$\frac{1}{j} = \frac{1}{j_L} + \frac{1}{j_k} = \frac{1}{j_k} + \frac{1}{B\omega^{1/2}} \quad (1)$$

Where j is the measured current density and j_k is the kinetic current density, respectively. ω is the electrode rotating rate. B is determined from the slope of the Koutechy-Levich (K-L) plots based on the Levich equation (**Equation 2**):

$$B = 0.2nFC_0D_0^{2/3}\gamma^{-1/6} \quad (2)$$

For **Equation** (**2**), n is the number of electrons transferred per oxygen molecule, F the Faraday constant (96485 C mol^{-1}), C_0 the bulk concentration of O_2 ($1.1*10^{-3}$ mol L^{-3}), D_0 the diffusion coefficient of O_2 in 0.1 M KOH ($1.9*10^{-5}$ cm^{-2} s^{-1}) and γ the kinetic viscosity of the electrolyte (0.01 cm^2 s^{-1})[7a]. The constant 0.2 is adopted if the rotation rate is expressed in rpm.

4.5. Fabrication of Co-N/C oxygen reduction reaction electrocatalyst.

4.5.1 Synthesis of Poly (AA-AM) Superabsorbent resin.

3D low cross-linking Poly (AA-AM) was first prepared by radical polymerization with the aid of the coupling agent, *N*,*N*-methylene diacrylamide.[35] Throughout this work, the AA/AM ratio of Poly (AA-AM) superabsorbent used in experiments was 7:3.

4.5.2 Synthesis of Co-N-C.

Herein, the synthesis process of cobalt, nitrogen-doped carbon materials Co-N-C is illustrated in **Figure 1**. Firstly, cobalt ions were embedded in cross-linking Poly (AA-AM) superabsorbent resin by easy adsorption. Several mg of Cobalt (II) acetate $C_4H_6O_4$ Co $4H_2O$ was dissolved in 10 ml of deionized water. Then 0.5 g as-prepared super absorbent resin was added into the above solution. The solid-liquid mixture was kept at room temperature for 1h. The obtained products displayed a similar polyhedron shape but a different colour (pink) to pure hydrogels.

After that, the prepared hybrid hydrogel was frozen by liquid nitrogen and freeze-dried at -45 ℃ in a vacuum lyophilizer for 24 h. Subsequently, the dried mixture were calcined under an argon atmosphere in a tube furnace at certain temperature for 2h with a heating ramp of 5 ℃ min^{-1}, and then furnace cooled down to room temperature. After ball milling with ethanol for 8h, the obtained products were purified by centrifugation and finally dried at 80 ℃.

To study the effects of the pyrolysis temperature and the cobalt element content on the catalytic activities, seven kinds of Co-N-C catalysts were prepared using the same method except for the difference of pyrolysis temperature or metal content. They were named like 800-2 Co-N-C catalyst, which "800" means the temperature of pyrolysis, and "2" represents the mass percentage of element cobalt in the as-prepared precursor solution and the resin.

Supporting Information

Supporting Information is available from the Wiley Online Library.

Acknowledgements

This work was financially supported by the National Materials Genome Project (2016YFB0700600), Shenzhen Science and Technology Research Grant (GJHZ20160229122304608).

Received: ((will be filled in by the editorial staff))
Revised: ((will be filled in by the editorial staff))
Published online: ((will be filled in by the editorial staff))

References

[1] a) A. Mahmood, W. Guo, H. Tabassum, R. Zou, *Adv. Energy Mater.* **2016**, 6, 1600423; b) A. Shen, Y. Zou, Q. Wang, R. A. Dryfe, X. Huang, S. Dou, L. Dai, S. Wang, *Angew. Chem., Int. Ed. Engl.* **2014**, 53, 10804-10808; c) I. T. Kim, M. J. Song, Y. B. Kim, M. W. Shin, *Int. J. Hydrogen Energy* **2016**, 41, 22026-22033.

[2] a) W. Xia, A. Mahmood, Z. Liang, R. Zou, S. Guo, *Angew. Chem., Int. Ed. Engl.* **2016**, 55, 2650-2676; b) J. Lee, B. Jeong, J. D. Ocon, *Curr. Appl. Phys.* **2013**, 13, 309-321.

[3] a) M. Kuang, Q. Wang, P. Han, G. Zheng, *Adv. Energy Mater.* **2017**, 7, 1700193; b) H.-x. Zhong, J. Wang, Y.-w. Zhang, W.-l. Xu, W. Xing, D. Xu, Y.-f. Zhang, X.-b. Zhang, *Angew. Chem., Int. Ed. Engl.* **2014**, 53, 14235-14239; c) Y. Qiu, J. Huo, F. Jia, B. H. Shanks, W. Li, *J. Mater. Chem. A* **2016**, 4, 83-95.

[4] a) Y. Zhou, K. Neyerlin, T. S. Olson, S. Pylypenko, J. Bult, H. N. Dinh, T. Gennett, Z. Shao, R. O'Hayre, *Energy Environ. Sci.* **2010**, 3, 1437-1446; b) R. Zhang, Y. Li, L. Liu, M. Jiang, W. Wang, *Ionics* **2017**, 23, 1849-1859.

[5] a) L. Wang, Z. Tang, W. Yan, Q. Wang, H. Yang, S. Chen, *J. Power Sources* **2017**, 343, 458-466; b) T. Toda, H. Igarashi, H. Uchida, M. Watanabe, *J. Electrochem. Soc.* **1999**, 146, 3750-3756; c) S. Liu, I. S. Amiinu, X. Liu, J. Zhang, M. Bao, T. Meng, S. Mu, *Chem. Eng. J.* **2018**, 342, 163-170.

[6] L. Yang, S. Jiang, Y. Zhao, L. Zhu, S. Chen, X. Wang, Q. Wu, J. Ma, Y. Ma, Z. Hu, *Angew. Chem., Int. Ed. Engl.* **2011**, 50, 7132-7135.

[7] a) J. Gao, N. Ma, Y. Zheng, J. Zhang, J. Gui, C. Guo, H. An, X. Tan, Z. Yin, D. Ma, *ChemCatChem* **2017**, 9, 1601-1609; b) P. Subramanian, R. Mohan, A. Schechter, *ChemCatChem* **2017**, 9, 1969-1978.

[8] Y. Dong, Y. Deng, J. Zeng, H. Song, S. Liao, *J. Mater. Chem. A* **2017**, 5, 5829-5837.

[9] J. Chen, N. Zhou, H. Wang, Z. Peng, H. Li, Y. Tang, K. Liu, *Chem. Commun.* **2015**, 51, 10123-10126.

[10] S. Dou, L. Tao, J. Huo, S. Wang, L. Dai, *Energy Environ. Sci.* **2016**, 9, 1320-1326.

[11] a) Y. Tong, P. Chen, T. Zhou, K. Xu, W. Chu, C. Wu, Y. Xie, *Angew. Chem., Int. Ed. Engl.* **2017**, 56, 7121-7125; b) C. H. Choi, M. W. Chung, S. H. Park, S. I. Woo, *Phys. Chem. Chem. Phys.* **2013**, 15, 1802-1805.

[12] T. He, H. Xue, X. Wang, S. He, Y. Lei, Y. Zhang, R. Shen, Y. Zhang, J. Xiang, *Nanoscale* **2017**, 9, 8341-8348.

[13] P. H. Matter, E. Wang, M. Arias, E. J. Biddinger, U. S. Ozkan, *J. Phys. Chem. B* **2006**, 110, 18374-18384.

[14] a) X. Song, L. Guo, X. Liao, J. Liu, J. Sun, X. Li, *Small* **2017**, 13, 1700238; b) H. Huang, Q. Wang, Q. Wei, Y. Huang, *Int. J. Hydrogen Energy* **2015**, 40, 6072-6084.

[15] C. J. Shearer, A. Cherevan, D. Eder, *Adv. Mater.* **2014**, 26, 2295-2318.

[16] D. S. Choi, A. W. Robertson, J. H. Warner, S. O. Kim, H. Kim, *Adv. Mater.* **2016**, 28, 7115-7122.

[17] Z. S. Wu, S. Yang, Y. Sun, K. Parvez, X. Feng, K. Mullen, *J. Am. Chem. Soc.* **2012**, 134, 9082-9085.

[18] U. B. Nasini, V. Gopal Bairi, S. Kumar Ramasahayam, S. E. Bourdo, T. Viswanathan, A. U. Shaikh, *ChemElectroChem* **2014**, 1, 573-579.

[19] S. Chao, Q. Cui, Z. Bai, H. Yan, K. Wang, L. Yang, *Int. J. Hydrogen Energy* **2014**, 39, 14768-14776.

[20] Y.-P. Zhu, Y. Liu, Y.-P. Liu, T.-Z. Ren, G.-H. Du, T. Chen, Z.-Y. Yuan, *J. Mater. Chem. A* **2015**, 3, 11725-11729.

[21] S. Fu, C. Zhu, H. Li, D. Du, Y. Lin, *J. Mater. Chem. A* **2015**, 3, 12718-12722.

[22] R. Jasinski, *Nature* **1964**, 201, 1212-1213.

[23] a) L. Ding, J. Qiao, X. Dai, J. Zhang, J. Zhang, B. Tian, *Int. J. Hydrogen Energy* **2012**, 37, 14103-14113; b) W. Li, A. Yu, D. C. Higgins, B. G. Llanos, Z. Chen, *J. Am. Chem. Soc.* **2010**, 132, 17056-17058.

[24] M. Jahan, Q. Bao, K. P. Loh, *J. Am. Chem. Soc.* **2012**, 134, 6707-6713.

[25] H.-C. Huang, I. Shown, S.-T. Chang, H.-C. Hsu, H.-Y. Du, M.-C. Kuo, K.-T. Wong, S.-F. Wang, C.-H. Wang, L.-C. Chen, K.-H. Chen, *Adv. Funct. Mater.* **2012**, 22, 3500-3508.

[26] Y. Wang, J. Yang, R. Du, L. Chen, *ACS Appl. Mater. Interfaces* **2017**, 9, 23731-23740.

[27] R. Bashyam, P. Zelenay, *Nature* **2006**, 443, 63-66.

[28] G. Wu, K. L. More, C. M. Johnston, P. Zelenay, *Science* **2011**, 332, 443-447.

[29] J. Gao, N. Ma, J. Zhai, T. Li, W. Qin, T. Zhang, Z. Yin, *Ind. Eng. Chem. Res.* **2015**, 54, 7984-7989.

[30] J. Masa, W. Xia, M. Muhler, W. Schuhmann, *Angew. Chem., Int. Ed. Engl.* **2015**, 54, 10102-10120.

[31] Y. Qian, Z. Liu, H. Zhang, P. Wu, C. Cai, *ACS Appl. Mater. Interfaces* **2016**, 8, 32875-32886.

[32] J. Zhang, H. Zhou, X. Liu, J. Zhang, T. Peng, J. Yang, Y. Huang, S. Mu, *J. Mater. Chem. A* **2016**, 4, 15870-15879.
[33] K. Lee, L. Zhang, H. Lui, R. Hui, Z. Shi, J. Zhang, *Electrochim. Acta* **2009**, 54, 4704-4711.
[34] X. Liu, I. S. Amiinu, S. Liu, K. Cheng, S. Mu, *Nanoscale* **2016**, 8, 13311-13320.
[35] H. Lin, *J. Wuyi Univ., Nat. Sci. Ed.* **2016**, 35, 6-10.

WILEY-VCH

Figure 1. Schematic illustration of the preparation procedure and ORR process of the Co-N-C catalyst.

WILEY-VCH

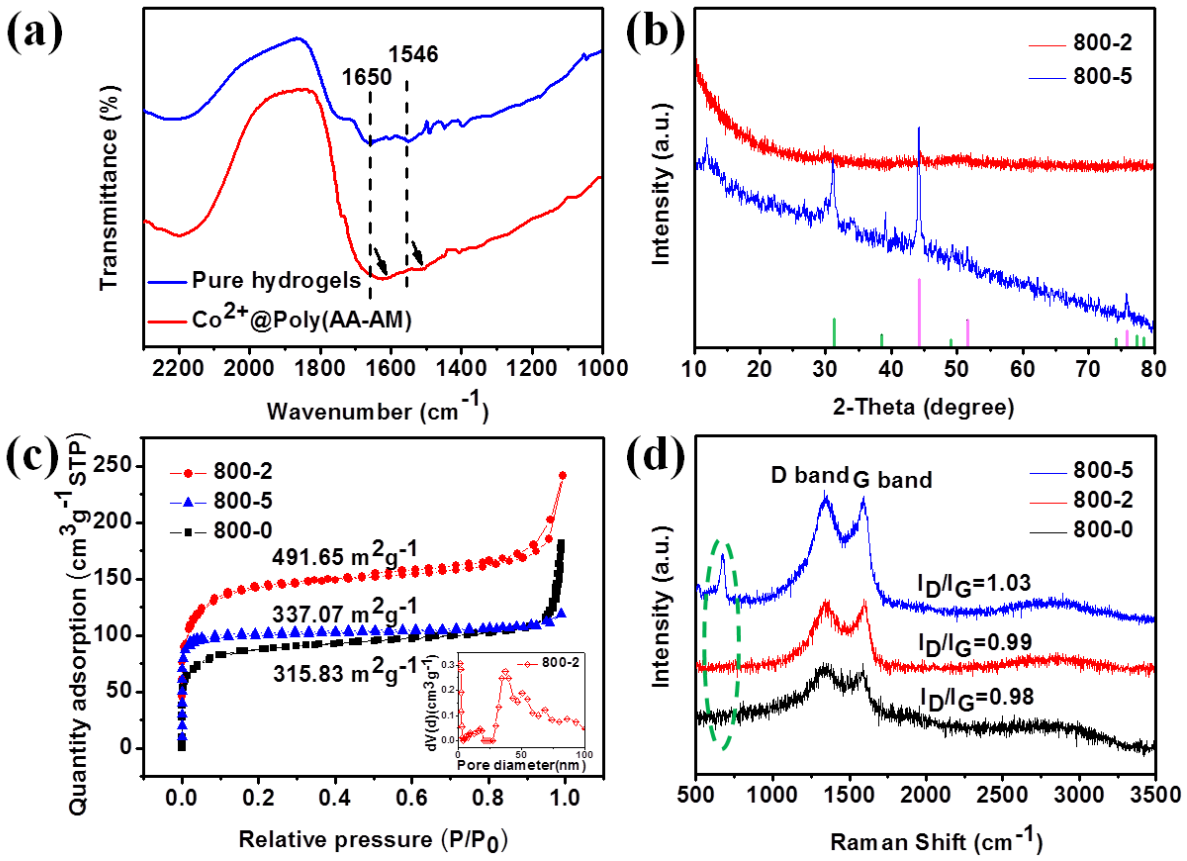

Figure 2. (a) FT-IR spectra of pure hydrogels Poly (AA-AM) and Co^{2+}@Poly (AA-AM). (b) XRD patterns of 800-2 and 800-5 Co-N-C catalysts. (c) Nitrogen adsorption-desorption isotherms and (d) Raman spectra of 800-0, 800-2 and 800-5 Co-N-C catalysts; the inset of (c) shows the pore size distribution of 800-2 Co-N-C catalysts.

WILEY-VCH

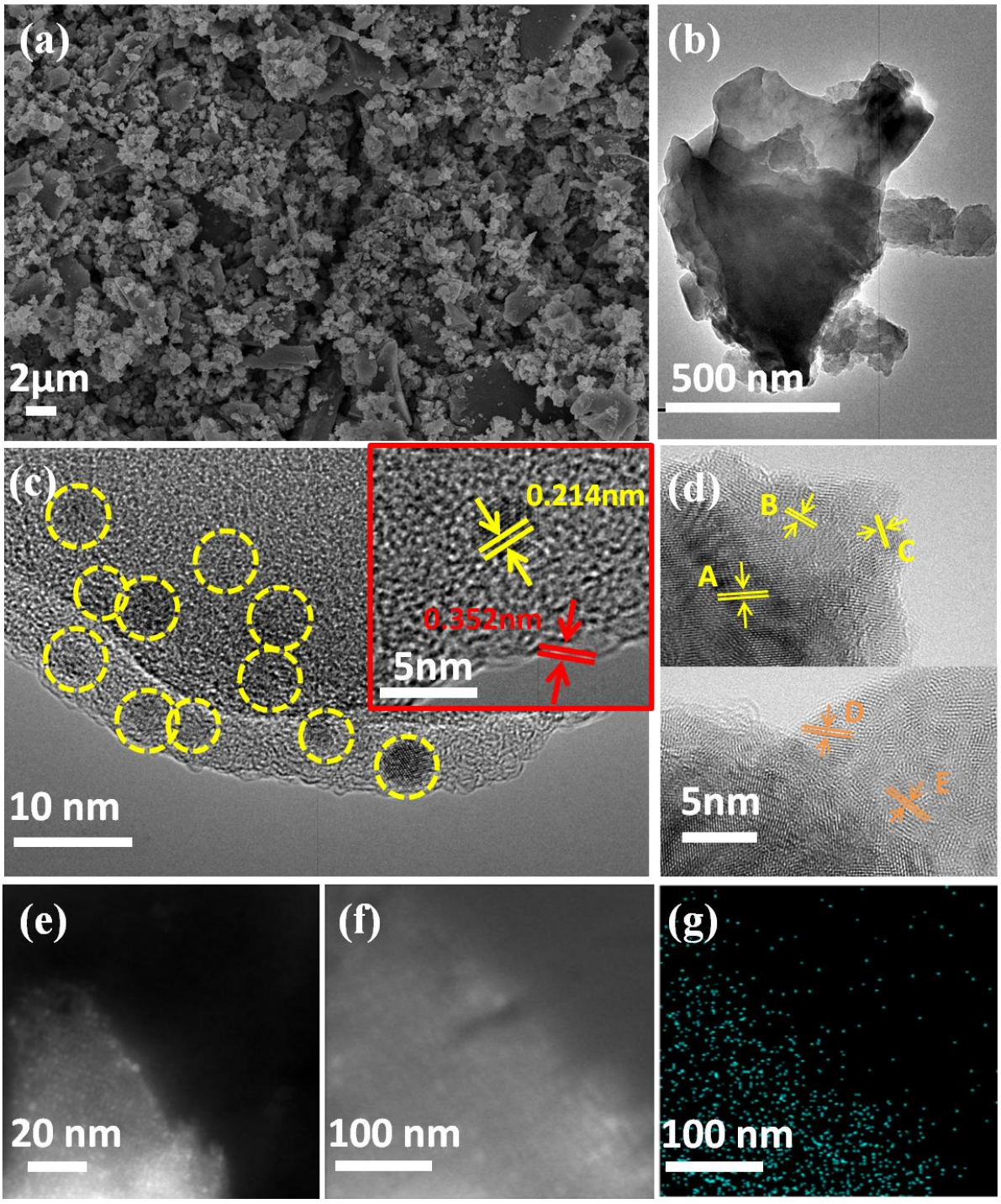

Figure 3. (a) SEM image and (b) TEM image of 800-2 Co-N-C catalyst. HRTEM images of 800-2 Co-N-C catalyst (c) and 800-5 Co-N-C catalyst (d). (e) HAADF-STEM image of 800-2 Co-N-C catalyst. And the corresponding elemental mapping for element Co (g) of a part of this region (f).

WILEY-VCH

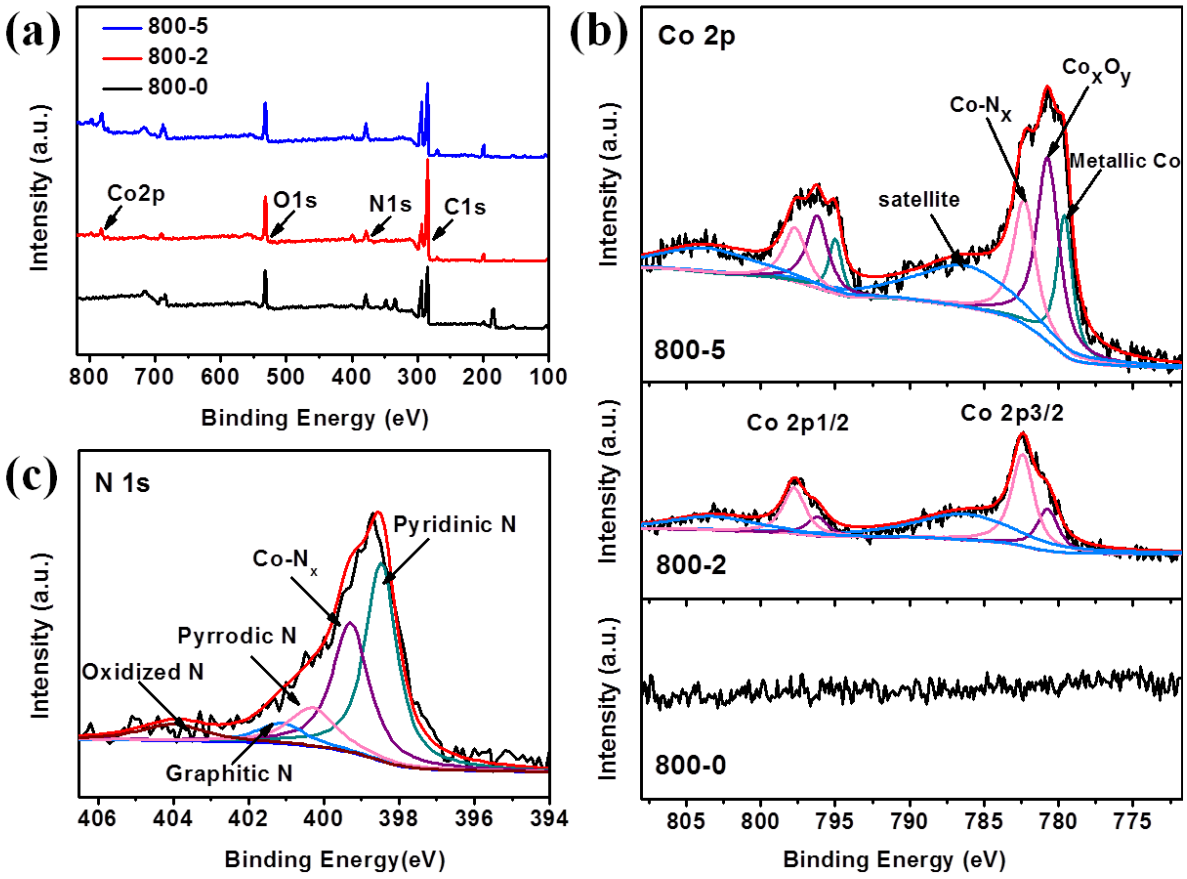

Figure 4. (a) XPS spectrums of 800-0, 800-2 and 800-5 Co-N-C catalysts. High-resolution XPS spectra of the Co 2p of 800-0, 800-2 and 800-5 Co-N-C catalysts (b) and the N 1s of 800-2 Co-N-C catalyst (c).

WILEY-VCH

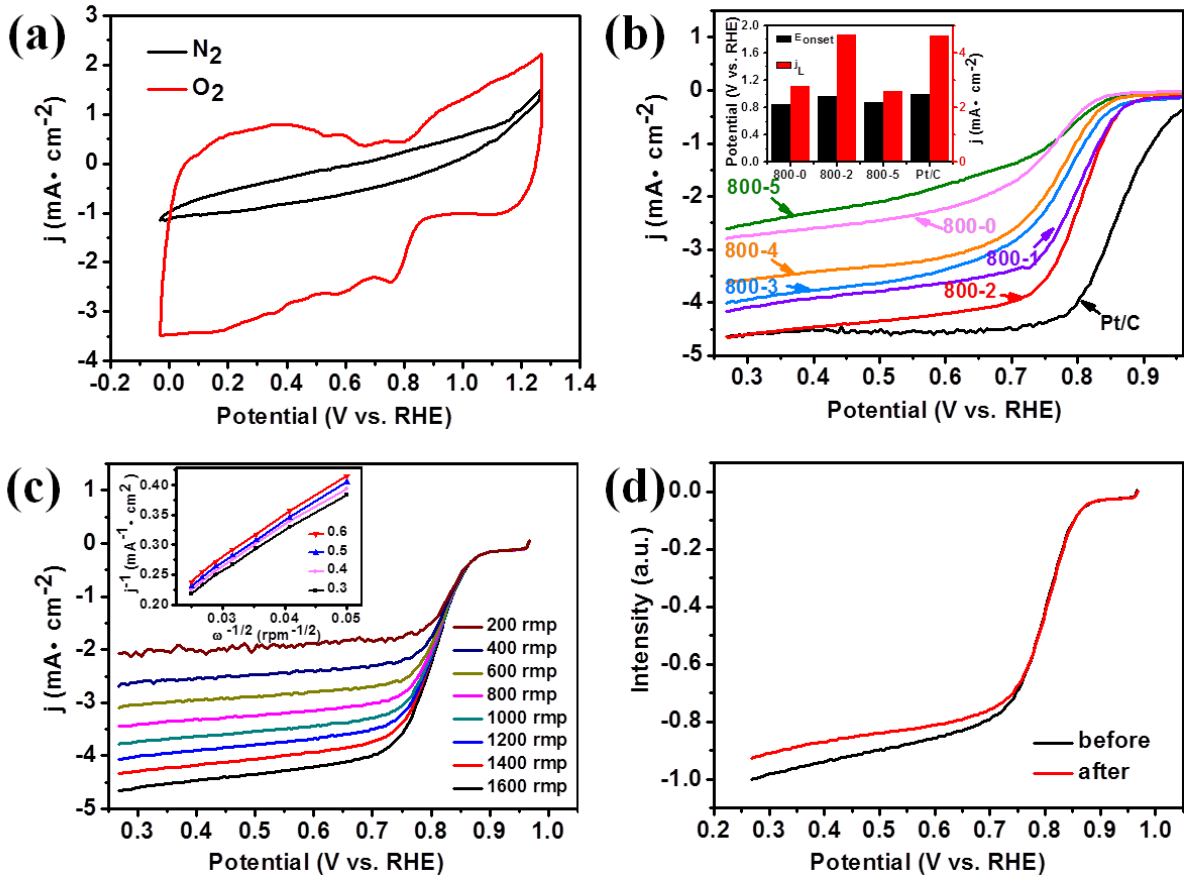

Figure 5. (a) CV curves for 800-2 Co-N-C catalyst at a sweep rate of 10 mV s^{-1} in N_2 and O_2-saturated 0.1M KOH electrolytes, respectively. (b) LSV curves for 800-(0-5) Co-N-C catalysts at a sweep rate of 10 mV s^{-1} in an O_2-saturated 0.1M KOH electrolyte. (c) LSV curves for 800-2 Co-N-C catalyst at various rotation rates (values displayed in rpm) in an O_2-saturated 0.1M KOH electrolyte; the inset of (c) shows the corresponding K-L plots derived from the RDE data. (d) LSV curves of 800-2 Co-N-C catalyst before and after 2000 potential cycles, respectively.

WILEY-VCH

Table 1. ORR electrocatalytic performance parameters of 800-(0-5) Co-N-C- from LSV in alkaline media.

Catalyst Co/N-C)	E_{onset} [V vs. RHE]	$E_{1/2}$ [V vs. RHE]	Diffusion-limiting current [mA cm^{-2}]
800-0	0.85	0.74	2.79
800-1	0.95	0.80	4.17
800-2	0.96	0.80	4.65
800-3	0.96	0.76	4.01
800-4	0.88	0.76	3.63
800-5	0.87	0.76	2.61
Pt/C	0.99	0.86	4.64

WILEY-VCH

We find a universal dispersing technology using super absorbent resin adsorbing metal ion and follow pyrolysis strategy to fabricate Co-N-C catalyst for ORR. The resin provides framework and doping elements sources to form actives sites. The catalyst exhibits excellent electrocatalytic performance with super low cost, which makes the composite catalyst easy to achieve commercialization instead of Pt-based catalyst.

Keyword: transition metal-nitrogen doping carbon catalysts, oxygen reduction reaction, superabsorbent resin, cobalt content

By Mengran Liu, Hai Lin, Zongwei Mei, Jinlong Yang, Jie Lin, Yidong Liu, and Feng Pan**

Tuning cobalt and nitrogen co-doped carbon to maximum catalytic sites by diaper superabsorbent for efficient oxygen reduction